ISSN 1726-5479

SENSORS & TRANSDUCERS

vol. 141
6/12

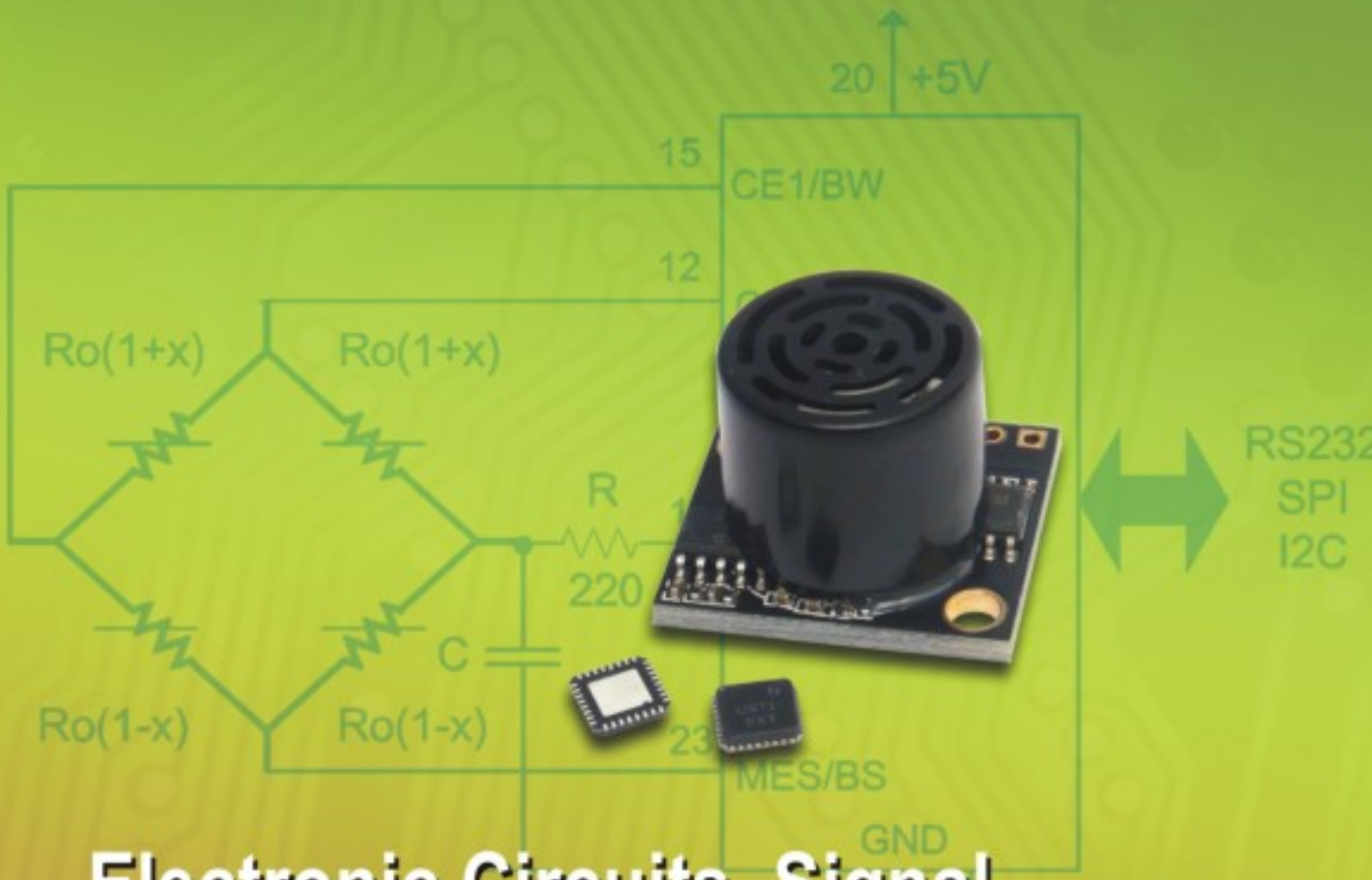

Electronic Circuits, Signal Conditioning and ASIC for Sensors

International Frequency Sensor Association Publishing

IFSA

Sensors & Transducers

Volume 141, Issue 6, June 2012 | **www.sensorsportal.com** | **ISSN 1726-5479**

Sensors & Transducers Journal (ISSN 1726-5479) is a peer review international journal published monthly online by International Frequency Sensor Association (IFSA).
Available in electronic and on CD.

Sensors & Transducers Journal

Contents

Volume 141
Issue 6
June 2012

www.sensorsportal.com

ISSN 1726-5479

Editorial

Research Articles

Authors are encouraged to submit article in MS Word (doc) and Acrobat (pdf) formats by e-mail: editor@sensorsportal.com
Please visit journal's webpage with preparation instructions: http://www.sensorsportal.com/HTML/DIGEST/Submition.htm

International Frequency Sensor Association (IFSA).

Sensors & Transducers Journal, Vol. 141, Issue 6, June 2012, pp. 106-118

www.sensorsportal.com

Sensors & Transducers

ISSN 1726-5479

http://www.sensorsportal.com

Analysis of the Self-Calibration Process in a Displacement Sensor in Applications of Hip or Knee Implants

Shiying Hao
Department of Biomedical Engineering, Institute of Orthopaedics and Musculoskeletal Science, University College London, UK
E-mail: s.hao@ucl.ac.uk.

Received: 10 June 2012 /Accepted: 25 June 2012 /Published: 30 June 2012

Abstract: An implantable displacement sensor for postoperative stability evaluation of THA (Total Hip Arthroplasty) or TKA (Total Knee Arthroplasty) implants proposed in our previous paper [5] features a self-calibrated algorithm to balance the DVRT bridge in the sensor before the measurement starts. The calibration process is accomplished by adjusting the frequency and phase of the output signal of the bridge iteratively until the bridge output is 0. Whether or not the calibration can be successfully accomplished depends on the errors of the intermediate parameter adjustments occurring in the calibration process. In this paper the influence of the frequency and phase adjustment errors on the calibration results is theoretically investigated. Simulation results indicate that such influence can be ignored given that the adjustment errors are in a specific range, and thus the calibration process can be simplified due to the high tolerance of the frequency adjustment error. Part of the hardware realization of the self-calibration process is also described in this paper and its feasibility is validated by the phase adjustment tolerance analysis. *Copyright © 2012 IFSA.*

Keywords: Displacement sensor, Calibration, Tolerance, Phase detector.

1. Introduction

The long term instability of the implants in total hip and knee arthroplasty (THA and TKA) has been noticed as a common problem in last few decades [1-4]. To estimate the postoperative instability of the implants before manufacture, in our previous paper a practical sensing method was developed to measure the postoperative *migration* (unrecoverable movement) and *micromotion* (recoverable movement) of an implant in vivo. The basic idea of this method is to use a DVRT (Differential Variable Reluctance Transducer) bridge with its inductance values changing with the implant position,

so that the implant *micromotion* can be detected by measuring the differential output voltage of the bridge. A self-calibration algorithm is also developed to balance the bridge initially before carrying out measurement, not only to improve the accuracy of subsequent *micromotion* measurement, but also to acquire the gross displacement (*migration*) of the implant since last phase.

As described in our previous study [5], in the calibration procedure, the operating frequency and the resistance values of the sensing bridge are adjusted iteratively to get a bridge phase shift of 0, 180º or ±90º until the output is zero. The features of the calibration enable itself to be realized in an automatic process in hardware, where a VCO oscillator with controllable frequency, a preamplifier and two phase detectors are needed. It should be noted that the errors of the oscillator frequency adjustment and phase detections must be small enough to ensure the convergence of the calibration process; otherwise the calibration may fail which will affect the accuracy of the subsequent displacement sensing. Therefore it is necessary to analyze the influence of the errors of the frequency adjustment and phase detection on the calibration process, which can be used to validate the hardware realization of the self-calibration process.

In this paper the frequency tolerance of the oscillator and the error tolerance of the phase detection to enable successful calibration are discussed. The design of the ±90° phase detector, as part of the hardware realization of the self-calibration process of the DVRT bridge, is also described. Testing results in combination with the phase detection tolerance analysis validate the feasibility of the phase detector.

Chapter 2 describes the DVRT bridge properties and the calibration process; in Chapter 3 the maximum allowable tolerances of the operating frequency and of the phase detection errors to enable a successful calibration are worked out by simulation; in Chapter 4 phase detector realization are presented and validated by comparing its testing results with the phase detection tolerances obtained in Chapter 3. Finally there are conclusions.

2. System Properties

The schematic of the system is shown in Fig. 1. The DVRT bridge consists of a pair of cylindrical inductive coils and two pairs of adjustable resistors. The inductance of the coils is changed by a ferrite rod moving along the coil axis. The ferrite rod is connected to the tip of the implant, while the coils are connected to the bone (a possible configuration for the implant in THA is shown in Fig. 2). The bridge is driven by a voltage controlled oscillator (VCO) of internal resistance r producing a sine wave of amplitude V_{in}, and (variable) frequency f.

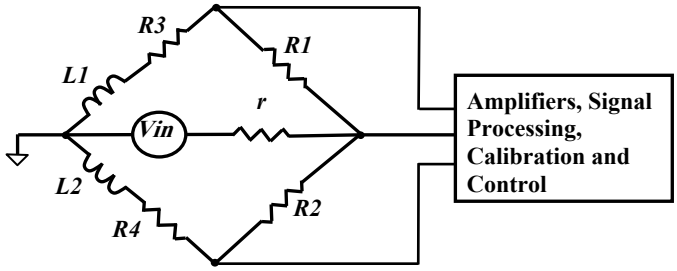

Fig. 1. Circuit schematic showing the form of the DVRT and its connection to the signal processing electronics (the series resistances of the coils are not shown in the figure).

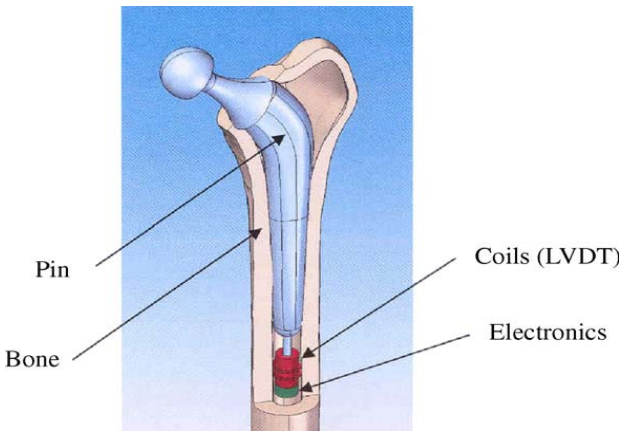

Fig. 2. Placement of the implanted DVRT, ferrite rod and electronics in *total hip arthroplasty* (THA).

The signal conditioning electronics includes amplification and bandpass filtering and also the feedback control circuitry that implements the self-calibration algorithm.

The bridge circuit is capable of measuring both *micromotion* (gross displacement) and *migration* (small displacement). The output differential voltage of the bridge circuit where the output has been nulled to zero when the rod has been placed at the exact geometrical centre of the coils is highly sensitive to small axial (z – direction) movement of the ferrite rod. Such motion (*micromotion*) can be calculated by dividing the change in output voltage by the gradient of the output voltage with respect to z at that point. On the other hand if, for some reason the system is not nulled initially, it will not be possible to calculate the gradient since the initial displacement from the null-point (*migration*) is not known. This is the usual situation encountered in practice. Unlike in most studies where a sensor bridge was calibrated by establishing a relationship between the output voltage and known input signal (e.g. position [6], force [7] et al.), a self-calibrated algorithm was described in [5] seeking to overcome this problem by effectively shifting the null point electronically.

If A_v is the voltage gain of the preamplifier, the overall transfer function of the system is:

$$H(j\omega) = A_v.H_1(j\omega) = A_v(REAL + j.IMAG) \tag{1}$$

This equation is the basis of the analysis of the self-calibration algorithm and described in some detail in reference [5]. To calibrate the bridge shown in Fig. 1, i.e. null the output to zero, the bridge is set initially so that $R_1 = R_2$ and $R_3 = R_4$. With reference to eqn. (1), the calibration procedure is as follows:

1. Sweep the oscillator frequency until the phase angle of $H_1(j\omega)$ is 0° or 180º. This is the resonant frequency of the system and sets the term *IMAG* in (1) to zero.
2. Adjust R_1 until the phase angle of $H_1(j\omega)$ is 90º or -90º. This sets the term *REAL* to zero.
3. Adjust R_3 until the phase angle of $H_1(j\omega)$ is 0° or 180º. This sets the term *IMAG* to zero.
4. Repeat steps 2 and 3 until the output is zero. In practice, the process is terminated when $|H_1(j\omega)|$ is less than a pre-determined threshold.

Not only does this calibration procedure restore the ability to calculate small axial shifts (*micromotion*), but also provides a means to calculate and record any large displacements (*migration*) since the last calibration by recording the calibrated value of R_1 and using a look-up table. Using this method it is possible to calculate *migration* and *micromotion* separately, a process which, as noted in reference [5] is somewhat analogous to large- and small-signal analysis in analogue circuit theory.

The implementation of the bridge on bench is described in [5]. The two coils L_1 and L_2 were realized with the dimensions given in Fig. 3, as required for a typical implant in THA or TKA. L_1 and L_2 each consisted of a 5-layer coil of 38 SWG insulated copper wire (about 400 turns in total) with a coupling coefficient k and series resistance r_L. The ferrite rod is a standard cylindrical component with a relative permeability (μ) of 48, resulting in a self-inductance of about 800 μH, mutual inductance of about 165 μH and series resistances of about 11 Ω. R1-4 are four 1 kΩ potentiometers with 0.1 Ω resolution. Initially, R_1 and R_2 were set to 400 Ω, R_3 and R_4 were set to 100 Ω, V_{in} = 0.1 V and f = 100 kHz. The gain of the preamplifier is 420, with 3dB bandwidth from 5 kHz to 120 kHz and a linear output from 0 to 500 mV. The threshold of $|H_1(j\omega)|$ to terminate the calibration process is 2.38×10^{-5}. The values of R_1 and R_3 after calibration are measured using a LCR meter, and the output voltage of the amplifier is observed using an oscilloscope.

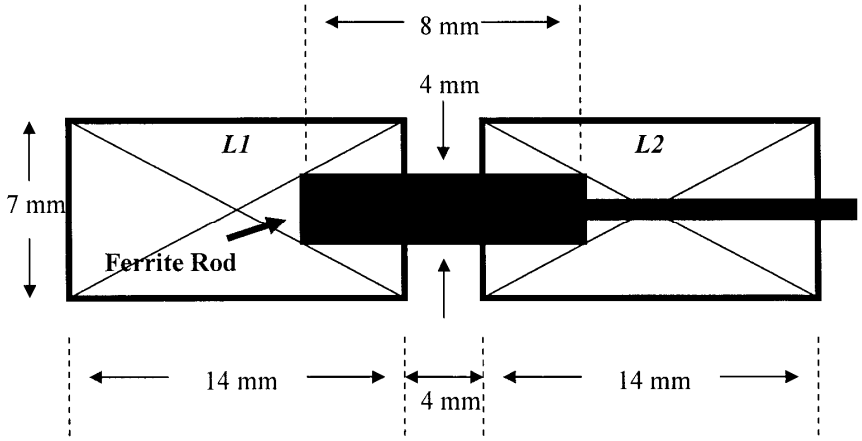

Fig. 3. Approximate coil and ferrite rod dimensions for use in THA.

In [5] the bridge was calibrated manually using potentiometers and an oscilloscope. However the nature of the calibration algorithm described above lends itself well to an automated realization using a microcontroller. This could be integrated with the rest of the electronics or alternatively kept separate and mounted on a small board. The main circuits/subsystems (in addition to the microcontroller) required in the design are (Fig. 4) (i) a voltage controlled oscillator (VCO), (ii) a preamplifier, (iii) a phase detector, (iv) a phase *quadrature* detector and (v) four variable resistors variable within the approximate range 100 Ω – 1 kΩ with a resolution of 0.1 Ω. This resolution can be obtained using a 16-bit A/D converter, which would be inexpensive and readily available.

To ensure the measurement accuracy of the displacement sensor, a successful calibration process is required in the full range of the initial axial displacement of the implant (between 0 and 4 mm). As described in the calibration procedures, the successful calibration depends on the convergence of the calibration process, which is highly correlated to the accuracy of the signal frequency adjustments and phase detections. In practice those adjustments can hardly be taken with 100 % accuracy. Therefore it is necessary to analyze the impacts of the frequency and phase errors on the calibration results, like the procedure convergence, the number of iterations taken in the procedure and the calibrated values of R_1 and R_3. These are discussed in Chapter 3, with a purpose of validating the part of the automatic calibration subsystem hardware design that is proposed in Chapter 4, and of simplifying the calibration process.

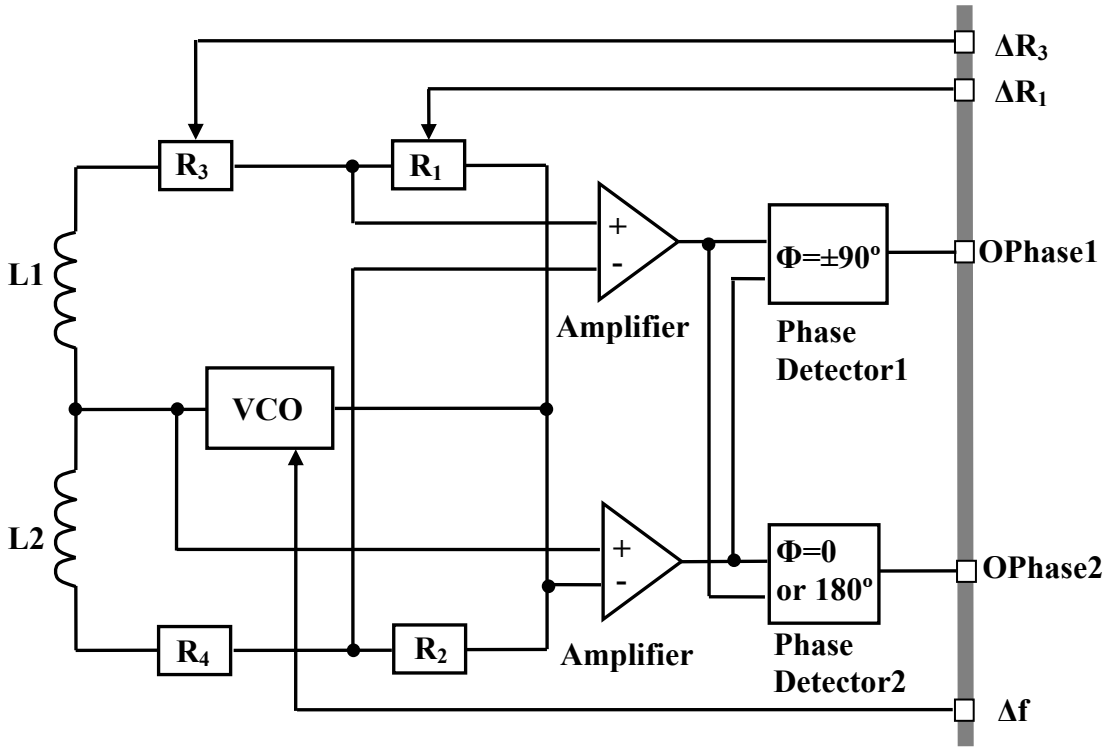

Fig. 4. Proposed hardware realization of the device. The component references correspond to Fig. 1 while the connections to the right of the figure are the microcontroller inputs and outputs.

3. Tolerance Analysis of Self-Calibration System

In this section the ranges of frequency and phase errors that allow a successful calibration process are discussed. Here are some definitions:

1. A successful calibration process is defined as a convergent calibration process with the number of iterations needed less than 10 and the errors of the final calibrated values of R_1 and R_3 less than 1 %;
2. The errors of the final calibrated values of R_1 and R_3 are defined as the differences between the theoretical and practical values of R_1 and R_3 after calibration;
3. Theoretical values of R_1 and R_3 after calibration are defined as the calibrated values of R_1 and R_3 with 100 % accuracy of frequency and phase adjustment during calibration procedure, while practical calibrated values of R_1 and R_3 are defined as the values of R_1 and R_3 got with some errors of those adjustments;
4. Frequency adjustment tolerance is defined as the maximum allowable difference between the practical and the theoretical calibrated oscillator frequencies that still enables a successful calibration;
5. Phase adjustment tolerance is defined as the maximum allowable phase detection errors of the 0/180º phase detector and of the ±90º phase detector that can still ensure a successful calibration.

All the analysis described in this section is made using a calibration algorithm model simulated in MatLab, based on the following initial conditions:

1. The shape of the coils and the rod are cylindrical and coaxial; The two coils are identical with each consisted of a 5-layer coil of 38 SWG insulated copper wire (about 400 turns in total); The relative permeability (μ) of the ferrite rod is 48; The dimension of the coils are shown in Fig. 3; The coil self-inductance and coupling coefficient k are 760 μH and 0.2 with the rod at centre.

2. $R_1 = R_2$, $R_3 = R_4$ initially and R_2 and R_4 are fixed during calibration; $R_1 + R_3 = R_2 + R_4 = 500$ Ω; The self-resistance of each coil is 10 Ω;
3. The source resistance r of the VCO is ignored.

3.1. Frequency Adjustment Tolerances Allowing Successful Calibration

The operating frequencies of the bridge after calibration as a function of the initial value of R_2/R_4 ($R_2 + R_4 = 500$ Ω) and the initial gross displacement of the implant (*migration*) are shown in Table 1. Table 1 illustrates that the calibrated frequency value ranges from 102 kHz to 109.6 kHz, which is irrespective of R_2/R_4.

The number of iterations needed in the calibration process and the errors of calibrated R_1 and R_3 as a function of the frequency adjustment errors are illustrated in Fig. 5a-c and Fig. 6a-c.

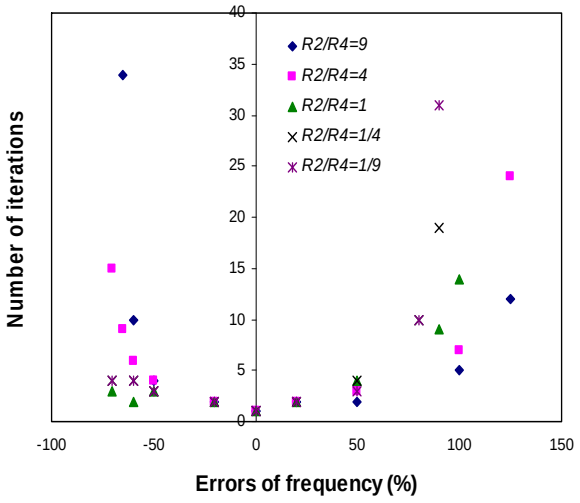

(a)

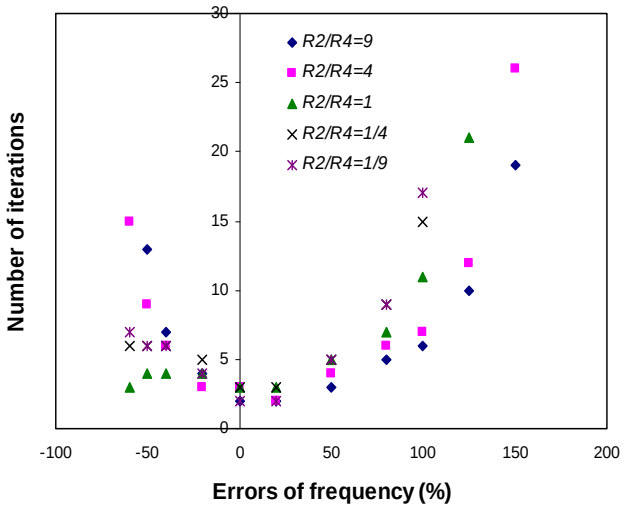

(b)

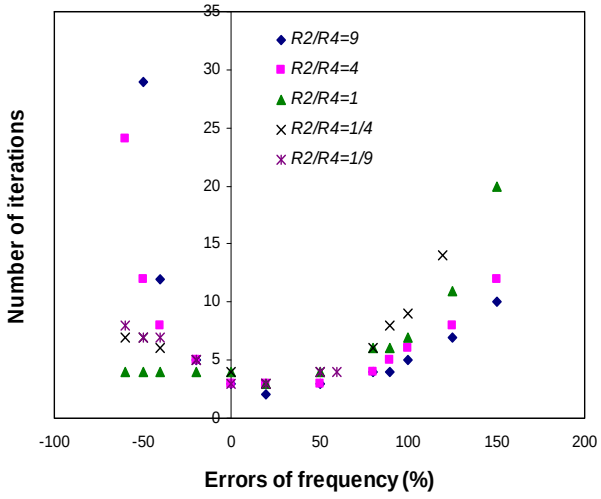

(c)

Fig. 5. The number of iterations in calibration process as a function of R_2/R_4 where $R_2 + R_4 = 500$ Ω at (a) $D = 0$, (b) $D = 2$ mm and (c) $D = 4$ mm.

Table 1. The operating frequency (kHz) of the DVRT bridge after calibration as a function of the initial migration D and R_2/R_4. $R_2 + R_4 = 500\ \Omega$.

D (μm)	R_2/R_4				
	1/9	1/4	1/1	4/1	9/1
0	109.6212	109.6212	109.6212	109.6212	109.6212
500	109.3099	109.3099	109.3099	109.3099	109.3099
1000	108.7969	108.7969	108.7969	108.7969	108.7969
1500	108.0758	108.0758	108.0758	108.0758	108.0758
2000	107.1673	107.1673	107.1673	107.1673	107.1673
2500	106.0866	106.0866	106.0866	106.0866	106.0866
3000	104.8133	104.8133	104.8133	104.8133	104.8133
3500	103.4421	103.4421	103.4421	103.4421	103.4421
4000	101.9925	101.9925	101.9925	101.9925	101.9925

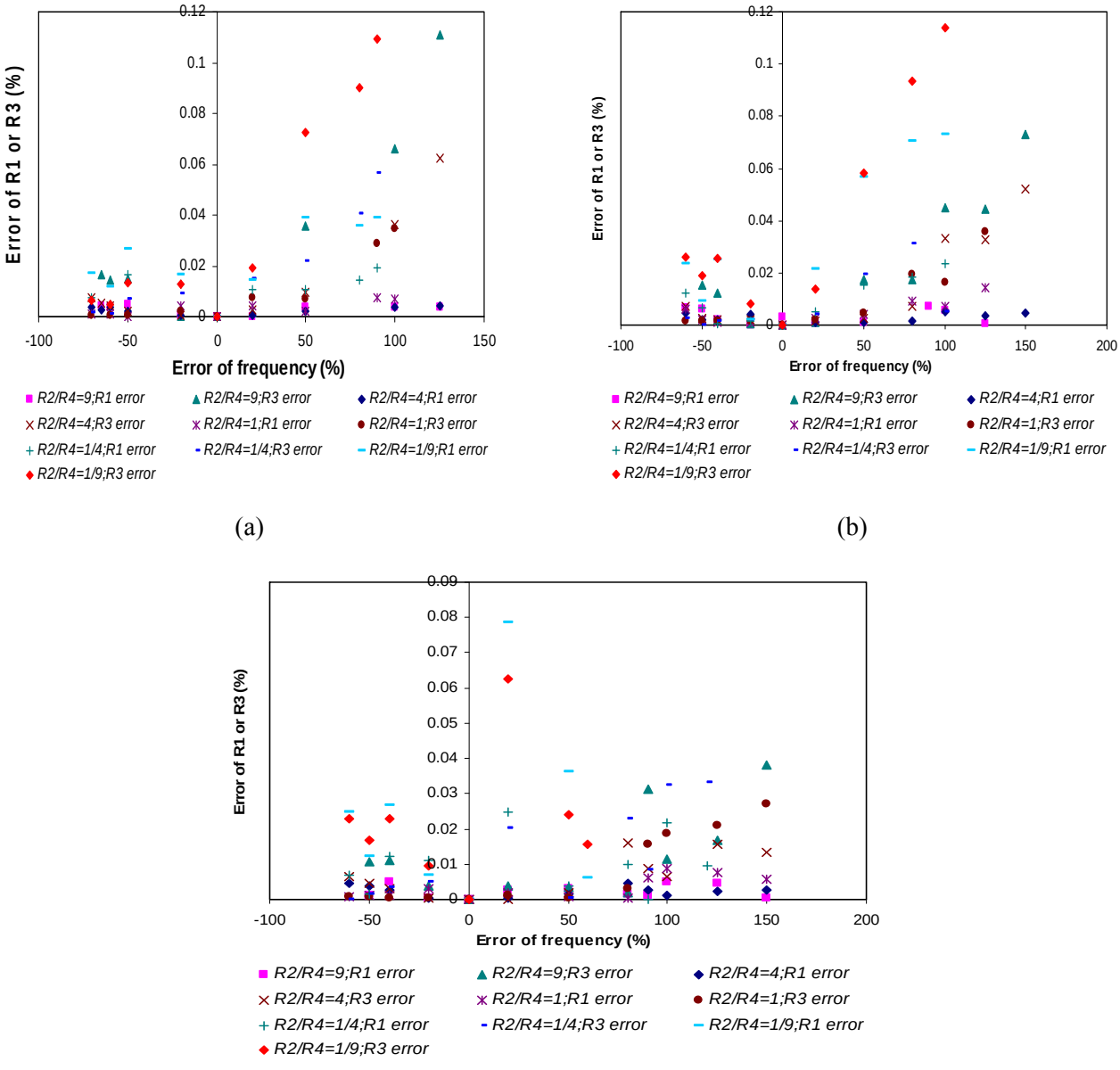

Fig. 6. Errors of the calibrated values of R_1 and R_3 as a function of R_2/R_4 where $R_2 + R_4 = 500\ \Omega$ at (a) $D = 0$, (b) $D = 2$ mm and (c) $D = 4$ mm.

As shown in these figures, with the frequency adjustment errors between ±50 %, the numbers of iteration needed for calibration are always less than 10 and the errors of calibrated $R_{1,3}$ values are always less than 1 % with initial migration D of 0, 2 and 4 mm. According to the definition of a successful calibration process, the calibration can always be considered successful as long as the error between the practical and theoretical frequencies is no more than ±50 %. Such huge tolerance of the frequency adjustment means that the influence of the frequency errors on the final calibration result is not very significant. As a result, the first step of the calibration process – adjusting the operating frequency of the bridge – is not necessary. Instead, the frequency can be set to an approximate value which is in the range between ±50 % of all the possible frequency values with the initial migration between 0 and 4mm (Table 1). For example, the frequency can be set to 100 kHz. After that, the calibration process starts by adjusting R_1 and R_3 iteratively until the bridge is balanced.

3.2. Phase Adjustment Tolerances Allowing Successful Calibration

The phase adjustment errors are mainly caused by the phase detection errors of the 0/180º and ± 90° phase detectors. Assume that the phase detection error of the 0 or 180º phase detector is α, and the phase detection error of the ± 90º is β, then Eqn. (1) is modified as:

$$H_1(j\omega) = \cos\beta.REAL - \sin\beta.IMAG + j.(\cos\alpha.IMAG + \sin\alpha.REAL) \quad (2)$$

According to the analysis in Appendix, α and β won't change the final calibrated values of R_1 and R_3, as long as a) the calibration process is convergent, b) sinα and cosβ are not equal to zero in the meantime and c) cosα and sinβ are not equal to zero in the meantime.

What will change with α and β is the number of iterations N needed in the calibration process. It is obvious that α and β will increase N and may cause the process divergent at some particular values.

Tables 2a-e illustrate the ranges of β that ensures N<= 10, as a function of α and R_2/R_4, with f = 100 kHz and R_2+R_4=500 Ω. The range of β that ensures N <= 10 is inversely correlated to the range of α and D. As α and β respectively represent the phase detection errors in 0/180º phase detector and ±90º phase detector, the ranges of α and β that ensure a successful calibration (N <= 10) with D ranging from 0 to 4 mm must be both fairly large, so that large detection tolerance is allowed for both phase detectors in the calibration. Thus, to determine the ranges of α and β a compromise is made here. The final optimum ranges of α and β that allow N <= 10 with the initial migration D from 0 to 4 mm are shown in Table 3. According to the definitions of the phase adjustment tolerances and a successful calibration, the values of α and β illustrated in Table 3 represent the tolerances of detection errors of 0/180º and ±90º phase detectors allowing a successful calibration. Table 3 also illustrates that the optimum ranges of both α and β are achieved when R_2/R_4 =1. i.e. R_2 = R_4 = 250 Ω, because the ranges of α and β are both large with those values.

4. Design and Testing Results of ± 90º Phase Detector

So far two ± 90º phase detectors have been designed using 0.35 μm and 0.8 μm CMOS technology respectively and tested. The block diagram and schematics are shown in Figs. 7 and 8a-d. The schematic of 0.35 and 0.8 μm phase detector are identical. As shown in Fig. 7, the detector consists of two channels with identical structure except for a capacitor C_p applied to produce 90° phase shift in one channel, while a resistor R_p applied to produce 0° phase shift in the other. Amplifiers and inverters are connected to both channels to convert the sine wave signals to square wave. Finally a D-type flip flop is connected to the output of both channels, with the data input connected to the capacitor channel and the clock input connected to the resistor channel.

Table 2. The range of β that ensures $N <= 10$ as a function of the range of α and D. $R_2 + R_4 = 500\ \Omega$. $f = 100$ kHz. (a) R_2/R_4=1/9, (b) R_2/R_4=1/4, (c) R_2/R_4=1/1, (d) R_2/R_4= 4/1, (e) R_2/R_4=9/1.

(a)

Range of α (°)	***D* (mm)**				
	0	**1**	**2**	**3**	**4**
-60~60	-20~20	-21~11	-22~4	-25~-3	-15~-7
-45~45	-24~32	-24~19	-27~15	-28~13	-17~12
-30~30	-27~45	-27~28	-29~24	-31~21	-19~17
-20~20	-30~53	-29~36	-31~31	-33~28	-21~26
-10~10	-32~63	-30~45	-33~40	-35~37	-24~34

(b)

Range of α (°)	***D* (mm)**				
	0	**1**	**2**	**3**	**4**
-60~60	-20~19	-21~9	-21~1	-22~-4	-22~-8
-45~45	-24~30	-25~17	-26~14	-29~11	-28~10
-30~30	-28~42	-28~27	-30~22	-32~20	-32~18
-20~20	-31~51	-30~34	-32~30	-34~27	-35~25
-10~10	-33~61	-32~44	-34~39	-36~36	-37~34

(c)

Range of α (°)	***D* (mm)**				
	0	**1**	**2**	**3**	**4**
-60~60	-22~18	-20~5	-21~-2	-22~-6	-23~-9
-45~45	-28~29	-28~18	-31~15	-30~9	-31~5
-30~30	-34~42	-33~29	-33~25	-34~23	-39~21
-20~20	-37~52	-37~37	-39~35	-39~33	-42~31
-10~10	-43~63	-42~50	-44~48	-44~46	-47~45

(d)

Range of α (°)	***D* (mm)**				
	0	**1**	**2**	**3**	**4**
-60~60	-24~15	-20~3	-21~-6	-22~-8	-23~-11
-45~45	-36~32	-29~15	-30~8	-31~1	-31~-1
-30~30	-46~45	-43~34	-42~25	-42~18	-42~14
-20~20	-53~57	-53~48	-53~41	-52~34	-51~29
-10~10	-63~70	-65~65	-57~47	-65~56	-64~51

(e)

Range of α (°)	***D* (mm)**				
	0	**1**	**2**	**3**	**4**
-60~60	-24~14	-21~3	-21~-4	-22~-8	-23~-11
-45~45	-35~29	-31~14	-30~7	-30~2	-31~-2
-30~30	-51~47	-43~29	-39~20	-42~14	-42~10
-20~20	-62~60	-54~42	-39~20	-42~14	-42~10
-10~10	-74~73	-67~59	-64~49	-63~42	-61~36

Table 3. Ranges of α and β that always allow $N <= 10$ with D between 0 and 4 mm and with different R_2/R_4. $R_2 + R_4 = 500\ \Omega$. $f = 100$ kHz.

R_2/R_4	1/9	1/4	1/1	4/1	9/1
Range of α and β	-20º<α<20º -21º< β<26º	-30º<α<30º -32º< β<18º	-30º<α<30º -39º< β<21º	-20º<α<20º -51º< β<29º	-30º<α<30º -42º< β<10º

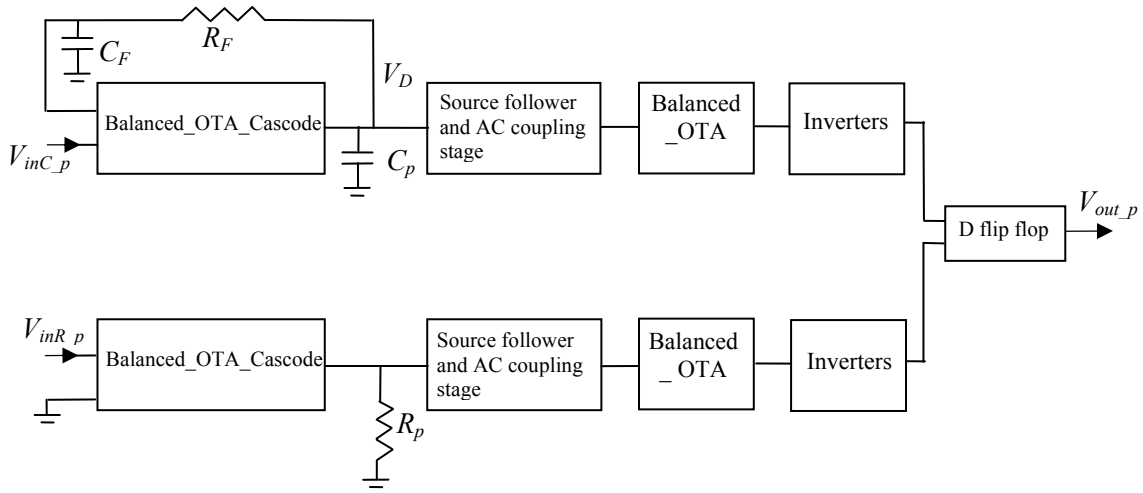

Fig. 7. Block diagram of the ±90° phase detector. R_F and C_F constitute a feedback system for signal stabilization in the capacitor channel. V_{inR_p} and V_{inC_p} are both sine wave signals. The DC supply is ± 1.5 V. The total power is approximate 0.45 mW. Circuit schematics for each block are shown in Figs. 8a-d.

The D flip flop is an electronic circuit having two stable states as its output always follows the state of the data input at the moment of a rising clock edge. Therefore, the output remains a low level when the phase difference between the inputs of two channels is between -90º and 90º, and a high level when the phase difference between the two inputs is between -180 º and -90 º or between 90 º and 180 º. As a result, the ± 90° phase difference at the inputs can be detected by means of level transition at the output of the flip flop. The photograph of the ± 90° phase detector chip is shown in Fig. 9.

Table 4 illustrates the phase detection errors. The input signal at each channel is 100 kHz sine wave signal with 0.1 V amplitude. Five chips for each CMOS technology were made and tested. It is apparent that the magnitudes of the phase detection errors in both phase detectors are less than 10º, which is in the range of the tolerance (as shown in Table 3) that guarantees a successful calibration for the DVRT bridge.

Table 4. Phase detection errors of the 0.35 μm and 0.8 μm ±90º phase detectors. $V_{in\_C} = V_{in\_R} = 100$ mV. $f = 100$ kHz.

CMOS technology	State transition	*Phase detection error* (º)				
		Chip 1	Chip 2	Chip 3	Chip 4	Chip 5
0.35 μm	Low level – High level	-5.0	-4.9	-6.0	-8.2	-4.2
	High level – Low level	-3.9	-3.5	-1.4	-0.2	-2.3
0.8 μm	Low level – High level	-4.1	-3.0	-1.0	-1.8	2.3
	High level – Low level	7.0	8.3	-3.8	0.9	2.1

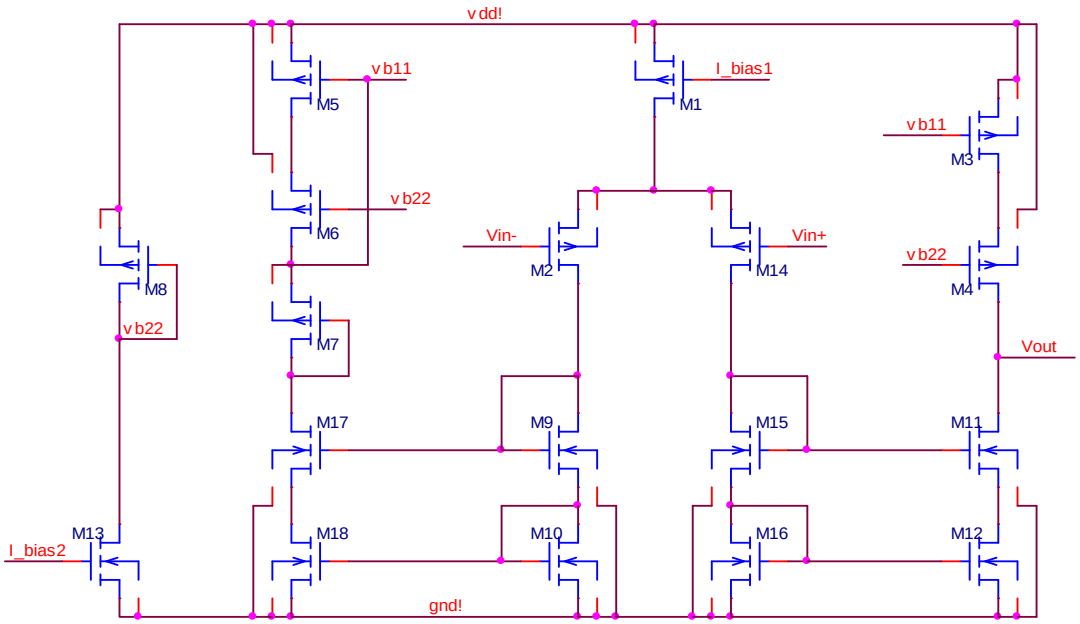

(a)

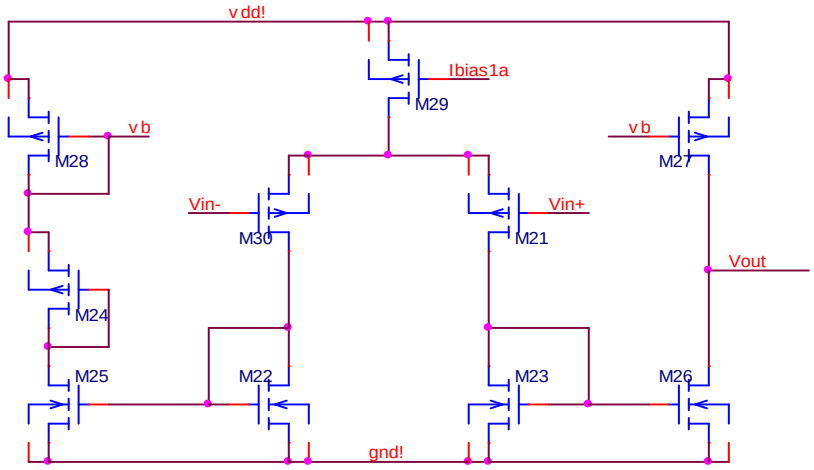

(b)

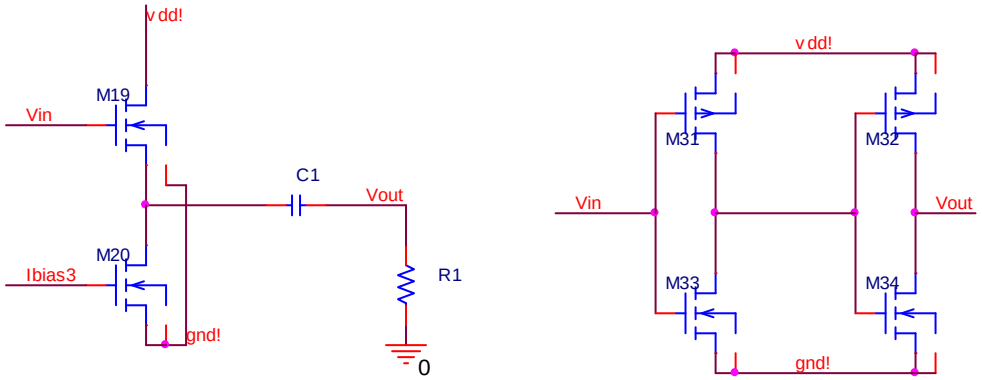

(c) (d)

Fig. 8(a)-(d). Schematic diagrams of (a) Balanced_OTA_Cascode; (b) Balanced_OTA; (c) Follower-Coupling, and (d) Inverter as shown in Fig. 7.

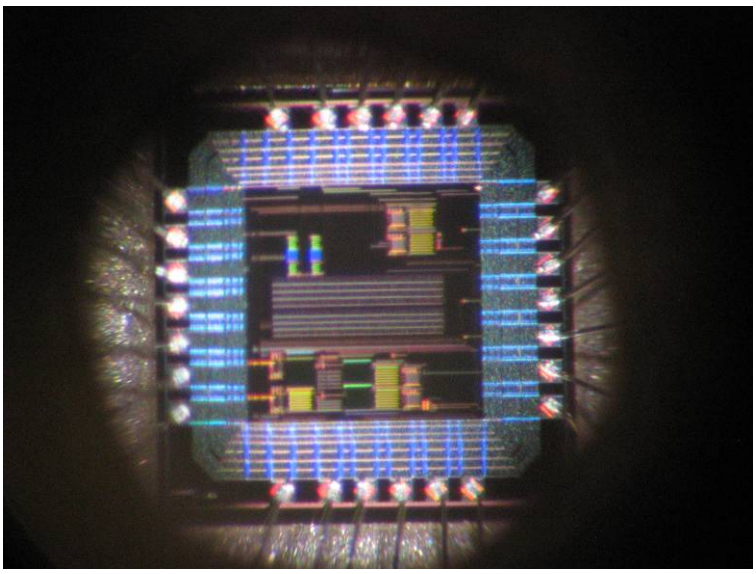

Fig. 9. Photograph of the phase detector chip. The area of the chip is 2.8 mm^2.

5. Conclusions

The tolerances of the signal frequency and phase shift adjustment errors in the calibration process of a DVRT bridge, which is the essential part of a displacement sensor designed for migration and micromotion measurement of THA or TKA implants, are analyzed in this paper. Simulation results show that with the coil model shown in Fig. 3, the frequency tolerance is large enough to bypass the frequency calibration. Instead the frequency can be fixed to 100 kHz, with the initial migration of the implant in a range between 0 and 4 mm. The tolerances of phase adjustment errors that allow a successful calibration are also calculated (Table 3), for both 0/180º phase detector and ±90º phase detector.

The measured results of the ±90º phase detector, realized in 0.35 μm and 0.8 μm CMOS technology respectively, illustrate that their phase detection errors are always less than the maximum tolerance shown in Table 3. As a result the design of the ±90º phase detectors is validated, and can be utilized as part of a self-calibration hardware system. The rest parts of the system will be designed and tested in the future.

Appendix

Modified Algorithm with Consideration of the Phase Detection Error of the Phase Detectors

Eqn. (1) describes the system without the consideration of the phase detection error. In that case, after calibration,

$$\begin{cases} REAL = 0 \\ IMAG = 0 \end{cases} \tag{A.1}$$

However in most cases the phase detection error needs to be considered. Assume that the 0/180º phase detector has a detection error of α, and the ±90º phase detector has a detection error of β, the transfer function shown in Eqn. (1) then can be modified as:

$$H_1(j\omega) = \cos\beta.REAL - \sin\beta.IMAG + j.(\cos\alpha.IMAG + \sin\alpha.REAL) \quad (A.2)$$

And after calibration

$$\begin{cases} \cos\beta.REAL - \sin\beta.IMAG = 0 \\ \cos\alpha.IMAG + \sin\alpha.REAL = 0 \end{cases} \quad (A.3)$$

The eqn. (A.3) is the sufficient and necessary condition of the eqn. (A.1) if $\alpha, \beta \neq \pm 90^o$ and tan $\alpha \neq$ ctg β. The relationship between eqn. (A.1) and (A.3) indicates the phase detector error doesn't affect the calibrated values of R_1 and R_3 as long as the calibration procedure is convergent.

References

[1]. M. D. Skolnick, M. B. Coventry and D. M. Ilstrup, Geomtric Total Knee Arthroplasty. A Two-Year Follow-up Study, *J. Bone and Joint Surg.,* Vol. 58-A, 1976, pp. 749-753.

[2]. E. Losina, J. Barrett, N. N. Mahomed, J. A. Baron and J. N. Katz, Early Failures of Total Hip Replacement: Effect of Surgeon Volume, *Arthritis & Rheumatism*, Vol. 50, 2008, pp. 1338-1343.

[3]. Janie T. Best, Revision Total Hip and Total Knee Arthroplasty, *Orthopaedic Nursing,* Vol. 24, No. 3, 2005, pp. 174-179.

[4]. H. U. Cameron and G. A. Hunter, Failure in Total Knee Arthroplasty: Mechanisms, Revisions, and Results, *Clin Orthop Relat Res.,* No. 170, 1982, pp. 141-146.

[5]. S. Hao et al., Sensing methodology for in vivo stability evaluation of total hip and knee arthroplasty, *Sensors and Actuators A-Physical,* Vol. 157, 2010, pp. 150-160.

[6]. Linear Variable Displacement Transducer (LVDT) Calibration Procedure (http://nees.org/data/get/facility/RPI/TrainingAndCertification/OnSiteProcedures/LVDT%20Calibration%20Procedure.pdf)

[7]. Connecting Strain Gauges and Shunt Resistors to the NI 9237 (http://digital.ni.com/public.nsf/allkb/892C84122A6501AE86257547007E5C53).

The 3rd International Conference on Sensor Device Technologies and Applications

SENSORDEVICES 2012

19 - 24 August 2012 - Rome, Italy

Deadline for papers: 5 April 2012

Tracks: Sensor devices - Ultrasonic and Piezosensors - Photonics - Infrared - Geosensors - Sensor device technologies - Sensors signal conditioning and interfacing circuits - Medical devices and sensors applications - Sensors domain-oriented devices, technologies, and applications - Sensor-based localization and tracking technologies

http://www.iaria.org/conferences2012/SENSORDEVICES12.html

The 6th International Conference on Sensor Technologies and Applications

SENSORCOMM 2012

19 - 24 August 2012 - Rome, Italy

Deadline for papers: 5 April 2012

Tracks: Architectures, protocols and algorithms of sensor networks - Energy, management and control of sensor networks - Resource allocation, services, QoS and fault tolerance in sensor networks - Performance, simulation and modelling of sensor networks - Security and monitoring of sensor networks - Sensor circuits and sensor devices - Radio issues in wireless sensor networks - Software, applications and programming of sensor networks - Data allocation and information in sensor networks - Deployments and implementations of sensor networks - Under water sensors and systems - Energy optimization in wireless sensor networks

http://www.iaria.org/conferences2012/SENSORCOMM12.html

The 5th International Conference on Advances in Circuits, Electronics and Micro-electronics

CENICS 2012

19 - 24 August 2012 - Rome, Italy

Deadline for papers: 5 April 2012

Tracks: Semiconductors and applications - Design, models and languages - Signal processing circuits - Arithmetic computational circuits - Microelectronics - Electronics technologies - Special circuits - Consumer electronics - Application-oriented electronics

http://www.iaria.org/conferences2012/CENICS12.html

Sensors & Transducers Journal

Guide for Contributors

Aims and Scope

Sensors & Transducers Journal (ISSN 1726-5479) provides an advanced forum for the science and technology of physical, chemical sensors and biosensors. It publishes state-of-the-art reviews, regular research and application specific papers, short notes, letters to Editor and sensors related books reviews as well as academic, practical and commercial information of interest to its readership. Because of it is a peer reviewed international journal, papers rapidly published in *Sensors & Transducers Journal* will receive a very high publicity. The journal is published monthly as twelve issues per year by International Frequency Sensor Association (IFSA). In additional, some special sponsored and conference issues published annually. *Sensors & Transducers Journal* is indexed and abstracted very quickly by Chemical Abstracts, IndexCopernicus Journals Master List, Open J-Gate, Google Scholar, etc. Since 2011 the journal is covered and indexed (including a Scopus, Embase, Engineering Village and Reaxys) in Elsevier products.

Topics Covered

Contributions are invited on all aspects of research, development and application of the science and technology of sensors, transducers and sensor instrumentations. Topics include, but are not restricted to:

- Physical, chemical and biosensors;
- Digital, frequency, period, duty-cycle, time interval, PWM, pulse number output sensors and transducers;
- Theory, principles, effects, design, standardization and modeling;
- Smart sensors and systems;
- Sensor instrumentation;
- Virtual instruments;
- Sensors interfaces, buses and networks;
- Signal processing;
- Frequency (period, duty-cycle)-to-digital converters, ADC;
- Technologies and materials;
- Nanosensors;
- Microsystems;
- Applications.

Submission of papers

Articles should be written in English. Authors are invited to submit by e-mail editor@sensorsportal.com 8-14 pages article (including abstract, illustrations (color or grayscale), photos and references) in both: MS Word (doc) and Acrobat (pdf) formats. Detailed preparation instructions, paper example and template of manuscript are available from the journal's webpage: http://www.sensorsportal.com/HTML/DIGEST/Submition.htm Authors must follow the instructions strictly when submitting their manuscripts.

Advertising Information

Advertising orders and enquires may be sent to sales@sensorsportal.com Please download also our media kit: http://www.sensorsportal.com/DOWNLOADS/Media_Kit_2012.pdf